physica status solidi rrl
www.pss-rapid.com

Increasing the Effective Area of Small-Sized CIGS Modules by Printed Ag Front Contacts

Katharina Gensowski, Timo Freund, Sebastian Tepner, and Florian Clement*

Despite the high-efficiency potential of the $Cu(In_{1-x}Ga_x)Se_2$ (CIGS) technology, its global market share is still relatively small. One reason for that is the comparatively low active module area caused by small cell widths and therefore the resulting amount of scribing lines for monolithic interconnection. This results in significant losses from cell-to-module level. One approach to overcome this issue is the application of front contacts. Throughout this study, the electrical performance of small-sized CIGS modules with cell widths of $w_c = 4$ mm, $w_c = 7$ mm, and $w_c = 17$ mm with and without front side metallization is evaluated. A low-temperature curing Ag paste is applied onto those different CIGS module designs by flatbed screen printing and parallel dispensing. The application of Ag-electrodes obtains a significant increase in module power of $\Delta P_{mmp,rel.} = +18\%$ for 4 mm cell widths compared to grid-free CIGS modules. Furthermore, the homogeneous electrode shape of dispensed structures enables broad cells of $w_c = 17$ mm in small-sized CIGS modules. As a result, the module performance increases by $\Delta P_{mmp,rel.} = +25\%$ compared to screen-printed Ag-electrodes, demonstrating the great potential of the dispensing approach for the CIGS technology and potentially other thin-film technologies.

1. Introduction

Thin-film solar cells are an innovative technology, particularly the $Cu(In_{1-x}Ga_x)Se_2$ (CIGS) solar cell concept, enabling further applications beyond the scope of conventional silicon photovoltaics. The thin material stack of CIGS solar cells can be either deposited on flexible, lightweight substrates like metal foils and polyimide foils or rigid glass substrates.[1–3] The back contacts of CIGS solar cells are realized by a molybdenum layer and the front contacts by a transparent conducting oxide (TCO) layer, typically by aluminum-doped zinc oxide layer. Between both contacts, there is the absorber (CIGS) and the buffer (CdS) material.[4] The annual worldwide production of CIGS modules is significantly limited, despite its versatile integration possibilities and high-efficiency potential.[5] Solar Frontier has presented a CIGS cell efficiency record of $\eta_{cell} = 23.35\%$ in 2019 cell area: 1 cm^2).[6] The CIGS module record of $\eta_{module} = 17.6\%$ has been presented on a large module area of 1.20 m × 0.60 m by NICE Solar Energy GmbH.[7] The significant cell-to-module losses are one of the main reasons for the low market share of this approach. The different aspects that lead to those apparent cell-to-module losses and potential approaches to decrease them have been summarized in the literature.[8] The resistive losses along the front contacts of the CIGS modules can be decreased, for instance, when exploiting the full potential of the TCO layer. Here, the monolithic interconnection is combined with highly conductive front electrodes. The metal grids act as front contacts of CIGS modules, ensuring an optimized current collection and thus improving the fill factor and resulting module power.[4,8–10] Hedayati et al. used different electrode materials on aluminum-doped zinc oxide layers like gold and graphene to simulate the corresponding *I–V* curves.[11]

Nowadays, the application of metal grids is merely common in silicon photovoltaics but not yet established on thin-film solar cells. The TCO layers are not conductive enough to allow wider cells than $w_c = 4$ mm in small-sized, grid-free CIGS modules without a significant decrease in module performances. Such designs of small-sized CIGS modules show an enormous amount of P1P2P3 interconnections, meaning the active module area is dramatically decreased and the dead area increased. Applying front contacts on top of TCO layers can overcome the limited electrical conductivity of these TCO layers. Front contacts enable designs of small-sized CIGS modules with wider cells than $w_c > 4$ mm resulting in larger active module areas due to fewer P1P2P3 interconnections. In this case, the TCO layers need no further adjustments in terms of their electrical conductivity.

Until now, there is no standard industrial metallization process for thin-film applications. Flatbed screen printing is the industry standard for applying line electrodes on silicon solar cells.[12,13] The question arises of which metallization techniques

K. Gensowski, S. Tepner, F. Clement
Production Technology – Structuring and Metallization
Fraunhofer Institute for Solar Energy Systems
Heidenhofstraße 2, 79110 Freiburg im Breisgau, Germany
E-mail: katharina.gensowski@ise.fraunhofer.de

T. Freund
NICE Solar Energy GmbH (former)
Alfred-Leikam-Straße 25, 74523 Schwäbisch Hall, Germany

The ORCID identification number(s) for the author(s) of this article can be found under https://doi.org/10.1002/pssr.202200040.

DOI: 10.1002/pssr.202200040

are suitable for CIGS modules, especially in the case of upscaling module sizes. On the R&D level, metal grids on CIGS substrates are realized by flatbed screen printing,[14–16] inkjet printing,[17,18] parallel dispensing,[19] and plating.[20] In addition, the metal grid design requires adaptations to realize optimal use of silver in terms of module power. The metal grid design is defined by the material stack of CIGS modules and their properties.[21,22]

Previously, Pospischil et al. have demonstrated the potential of parallel dispensing as a metallization printing process for different solar cell applications by achieving Ag-electrode widths below $w_{shading} = 20\,\mu m$.[23,24] The parallel dispensing technology is a direct writing printing method that applies paste threads contactless onto a substrate. Here, high viscous non-Newtonian suspensions are extruded through narrow nozzle openings below $D < 60\,\mu m$. Multinozzle print heads with up to 130 parallel nozzles guarantee high throughput rates, which are especially essential in the photovoltaic market.[25–27] Furthermore, the dispensing approach enables a very uniform narrow Ag-electrode shape which can be described by different geometrical parameters.[28] The maximum shaded area of the Ag-electrode including any spreading is represented by the shading electrode width $w_{shading}$. The core electrode width w_{core} is defined as the part of electrode width, which shows a significant line height, meaning that no paste spreading is included. The optical aspect ratio AR_o is calculated by the ratio of the maximum electrode height $h_{f,max}$ to the shading line width $w_{shading}$.[23]

The advantageous application of the dispensing process on CIGS substrates is depicted in **Figure 1** and has been presented in the study by Gensowski et al.[19]. Further, both scanning electron microscope (SEM) images in Figure 1 show a homogeneous Ag-electrode shape on CIGS substrates but paste-specific geometric dimensions result from different paste properties. The Ag-electrodes are applied perpendicular to the P1P2P3 interconnections.

In this study, we investigate the electrical performances of small-sized CIGS modules concerning three different cell widths w_c combined with the application of front contacts onto the indium tin oxide (ITO) layer. The cell widths are $w_c = 4.069$ mm, $w_c = 6.941$ mm, and $w_c = 16.857$ mm. We use flatbed screen printing and parallel dispensing as printing technologies to apply one low-temperature curing Ag paste. The metal grids are printed perpendicularly to the P1P2P3 interconnections.

2. Experimental Section

Figure 2 illustrates the experimental plan of our study in which metal grids are applied onto small-sized CIGS modules. In total, our study includes eleven experimental groups of transfer length method (TLM) CIGS substrates and small-sized CIGS modules. Each experimental group contains five (groups Gr.1 to Gr.3) or ten samples (groups Gr.4 to Gr.11). The glass substrate size is 156 mm × 156 mm with an aperture area of the CIGS substrate of $A_{aperture} = 157.30\,cm^2$. The CIGS modules differ in cell widths between $w_c = 4.069$ mm, $w_c = 6.941$ mm, and $w_c = 16.857$ mm, respectively. That means that the cell width defines the number of cells of a single small-sized CIGS module and thus also the areal percentage by scribing per module (**Table 1**). All material layers are deposited on 3 mm thick glass substrates using a sequential P1P2P3 patterned interconnection approach. The material stack of CIGS solar cells that we used in our study is depicted in **Figure 3**a. Further information about the stacking sequence Mo/CIGS/chemical bath deposition (CBD)-CdS/i-ZnO/ZnO:Al/ITO is presented in our previous study.[19] The P1P2P3 interconnection width is $w_{P1P2P3} = 300\,\mu m$ for all small-sized CIGS modules used in this study. It should be mentioned that industrial fabricated CIGS modules can show narrower scribing lines down to $w_{P1P2P3} = 150\,\mu m$.[16] Table 1 summarizes the data of scribing lines in detail.

The material stack Mo/CIGS/(CBD)-CdS/i-ZnO/ZnO:Al/ITO is full surface deposited on 3 mm thick glass substrates for TLM measurements. The molybdenum acts as the rear contact and is deposited as the first layer onto the glass. Thus, the stacking sequence for TLM substrates as well as for CIGS modules is equal, but TLM substrates have no P1P2P3 interconnections. The samples have been provided by NICE Solar Energy GmbH.

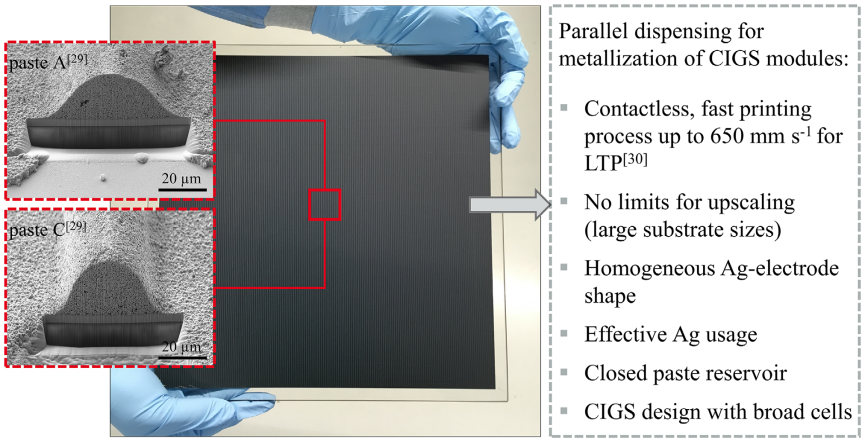

Figure 1. Ag-electrodes on small-sized CIGS modules and the beneficial properties of parallel dispensing for CIGS application. The Ag-electrodes and the P1P2P3 scribing lines are orientated perpendicular to each other. The SEM images are taken out of ref. [29] (paste A: $w_{shading} = (46 \pm 3)\,\mu m$, $w_{core} = (36 \pm 1)\,\mu m$, $AR_o = (0.38 \pm 0.02)$ | paste C: $w_{shading} = (41 \pm 3)\,\mu m$, $w_{core} = (25 \pm 1)\,\mu m$, $AR_o = (0.46 \pm 0.02)$). The feasible printing process up to $v_{process} = 650\,mm\,s^{-1}$ for low-temperature curing pastes (LTP) is shown in ref. [30].

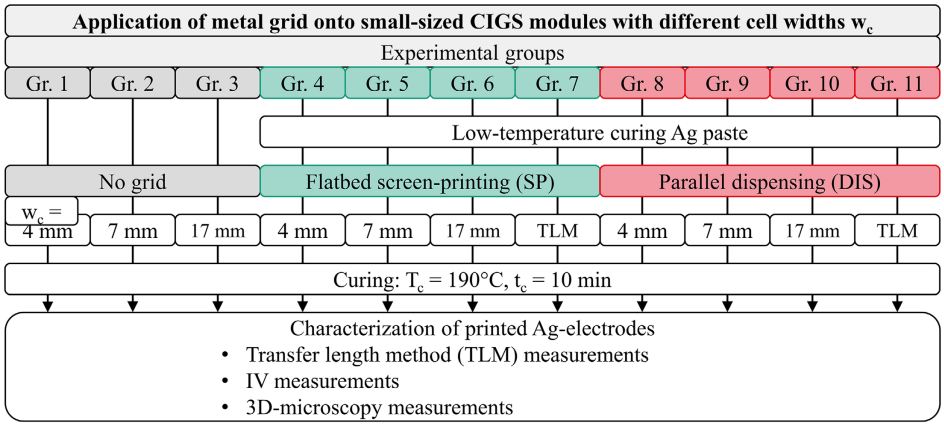

Figure 2. Experimental plan for applying metal grids onto small-sized CIGS substrates. A low-temperature curing Ag paste is printed by flatbed screen printing and parallel dispensing onto small-sized CIGS substrates. Small-sized CIGS modules differ in their cell widths of $w_c = 4.069$ mm, $w_c = 6.941$ mm, or $w_c = 16.857$ mm, respectively. Group Gr.1 to group Gr.3 are the reference groups, including grid-free CIGS modules. The curing temperature of $T_c = 190$ °C for $t_c = 10$ min is used for all samples. The Ag-electrode shape and the electrode performance of the small-sized CIGS modules are characterized.

Table 1. Details on architecture and P1P2P3 interconnection of small-sized CIGS modules with cell widths of $w_c = 4.069$ mm, $w_c = 6.941$ mm, and $w_c = 16.857$ mm. The glass substrates of these samples have an area of $A_{substrate} = 243.36\ cm^2$; the aperture area is $A_{aperture} = 157.30\ cm^2$. All small-sized CIGS modules show a broad interconnection width of $w_{P1P2P3} = 300$ µm, especially the pitch distance between P2 and P3 scribing. It should be noted that improved industrial configurations use interconnection widths down to $w_{P1P2P3} = 150$ µm.[16]

	Interconnection width w_{P1P2P3}				Small-sized CIGS modul with cell width w_c		
	Width [µm]	Pitch distance [µm]			4.069 mm	6.941 mm	16.857 mm
P1	60	–	Total cell number per module		29	17	7
P2	50	–	Cell length l_{cell} [mm]		130	130	130
P3	50	–	Ag-electrode width $w_{shading}$ [µm][a)]	SP	40	40	40
P1P2	–	30		DIS	57	57	57
P2P3	–	110	Active cell area (w/o dead area) A_{active} [cm^2]		4.90	8.63	21.52
P1P2P3	–	300	Active cell area (w/o dead area and front contacts) A_{active} [cm^2]	SP	4.74	8.35	20.85
				DIS	4.67	8.23	20.55
			Areal percentage by scribing per module A_{P1P2P3} [%][b)]		7.19	4.21	1.74
			Areal percentage by front contacts per module $A_{contacts}$ [%][b)]	SP	3.02	3.02	3.02
				DIS	4.33	4.33	4.33

[a)]Results are taken from Section 3 of this study. [b)]Related to functionalized module area $A_{aperture} = 157.30\ cm^2$.

In the present study, a low-temperature curing Ag paste is printed onto the ITO layer by flatbed screen printing and parallel dispensing. Typically, this paste is used for silicon heterojunction solar cells metallization and thus requires a curing temperature of $T_c = 200$ °C to form a sufficient electrically conductive contact. This highly filled suspension consists of an epoxy-phenolic resin system, solvents, and spherical Ag powder (particle sizes < 1 mm); the nonvolatile content is above 90% after the curing procedure.

The flatbed screen printing process is conducted at a semiautomatic EKRA XH STS screen printer. The principle of this printing technology is well described in the literature.[31,32] For this experiment, a screen with the specification of $360 \times 0.016 \times 22.5°$ was used. That means the screen has a mesh count of $MC = 360\ inch^{-1}$, is made of wires with a diameter of $d_{wire} = 16$ µm, and shows a screen angle of $\varphi = 22.5°$. The screen openings are $w_n = 33$ µm. The Ag-electrode pitch of the metal grid is 1.425 mm (Figure 3b). The squeegee pressure is set to $p_{squeegee} = 65\ N\ cm^{-1}$; further the squeegee is placed at an angle of $\theta = 60°$ to the screen. A constant flooding velocity of $v_{flooding} = 150\ mm\ s^{-1}$ as well as a constant printing velocity of $v_{printing} = 100\ mm\ s^{-1}$ is used.

The parallel dispensing process is performed at an R&D platform from ASYS Group (Dornstadt, Germany). Here, the low-temperature curing Ag paste is extruded via an R&D print head with 30 µm nozzle openings at room temperature. Eleven nozzles are arranged in parallel on the nozzle plate which is installed at the print head.[26] The Ag-electrode pitch of the metal grid is 1.413 mm. The R&D print head moves with a process velocity of $v_{process} = 100\ mm\ s^{-1}$ across the substrate surface. The distance between the nozzle plate and the sample is $d_{gap} = 500$ µm, following only the paste threads get in contact with the CIGS substrate.

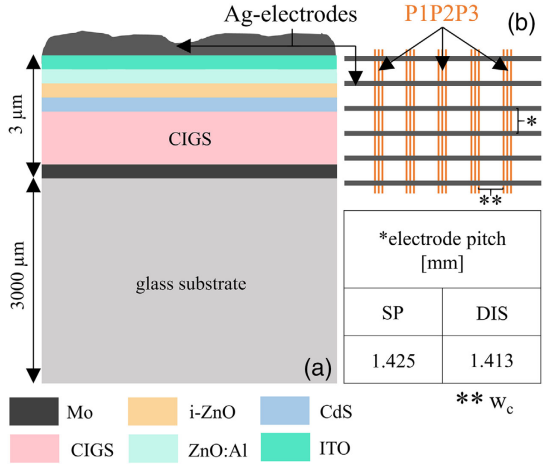

Figure 3. Schematic illustration of CIGS solar cell material stack and front contact metallization on ITO layer used in this experimental study. a) All layers are deposited on rigid glass substrates, whereby the molybdenum layer acts as back contact and the Ag-electrodes as front contact of the CIGS solar cells. The absorber material is the CIGS layer; the buffer layer is the CdS layer. b) The Ag-electrodes are applied vertically to the P1P2P3 interconnection onto a CIGS module. The cell width w_c refers to the distance between two interconnection areas; in this case, $w_c = 4.069$ mm, $w_c = 6.941$ mm, or $w_c = 16.857$ mm. Each P1P2P3 interconnection corresponds to a dead area of a module. The interconnection is 300 µm wide. The electrode-to-electrode distance is 1.425 mm for the screen printing (SP) layout and 1.413 mm for the dispensing (DIS) layout. Both schematics are not to scale.

After applying the paste by printing processes, the metal grids are cured in a continuous convection oven R0400FC from Essemtec AG (Switzerland) for $t_c = 10$ min. The curing temperature is set to $T_c = 190$ °C. The choice of these parameters is based on the findings in our previous experiments.[19] Subsequently, the metalized CIGS substrates are characterized regarding the achieved Ag-electrode shapes (3D-microscopy) and the electrical performances (TLM measurements, *I–V* measurements). The electrode width can be described by the shading electrode width $w_{shading}$ and the core electrode width w_{core}. The shading electrode width $w_{shading}$ corresponds to the maximum, shaded area of the Ag-electrode including any spreading. In contrast to that, the core electrode width w_{core} describes the part of electrode width which shows a significant electrode height, meaning that no paste spreading is included.[23] The metalized TLM substrates need to be mechanically separated into 10 mm wide stripes to perform the TLM measurements. The P3 scribing and fixing contact stripes to the CIGS modules are carried out before doing the *I–V* measurements at standard test conditions. The procedure of each characterization method is described in detail in the literature.[19]

3. Results and Discussion

The *I–V* parameters of the nonlaminated CIGS modules are estimated by using an h.a.l.m. flasher *I-V*-tool at standard test conditions. The measuring results are summarized in **Figure 4**. The grid-free CIGS modules with cell width of $w_c = 4.069$ mm (group Gr.1) achieve an average short-circuit current density of $j_{sc|Gr.1} = (31.6 \pm 0.1)$ mA cm^{-2} ($J_{sc,module|Gr.1} = (145 \pm 1)$ mA). Screen-printed and dispensed CIGS modules with the cell widths of $w_c = 4.069$ mm and $w_c = 6.941$ mm result in similar short-circuit current densities between $j_{sc|Gr.8} = (31.5 \pm 0.1)$ mA cm^{-2} and $j_{sc|Gr.5} = (32.2 \pm 0.2)$ mA cm^{-2}. The mean short-circuit current densities differ significantly for CIGS modules with cell widths of $w_c = 16.857$ mm. The short-circuit current density of grid-free CIGS modules (group Gr.3) is $j_{sc|Gr.3} = (14.5 \pm 1.1)$ mA cm^{-2} ($J_{sc,module|Gr.3} = (242 \pm 18)$ mA) which corresponds to losses of $\Delta j_{sc} = -17.1$ mA cm^{-2} compared to CIGS modules of group Gr.1. However, CIGS modules with screen-printed and dispensed metal grids show an increase of the short-circuit current density when using wider cells in the module. CIGS modules of group Gr.10 result in an average short-circuit current density of $j_{sc|Gr.10} = (38.5 \pm 0.3)$ mA cm^{-2} ($J_{sc,module|Gr.10} = (643 \pm 5)$ mA). The tendencies of the quantitative short-circuit current densities for groups Gr.6 and Gr.10 as well as the tendency of the short-circuit current density drop for group Gr.3 are not fully understood yet; therefore, further experiments are needed.

The grid-free CIGS modules of group Gr.1 have an average open-circuit voltage per cell of $V_{oc|Gr.1} = (711 \pm 4)$ mV cell^{-1} and an average open-circuit voltage per module of $V_{oc,module|Gr.1} = (20.62 \pm 0.11)$ V. The metalized CIGS modules of groups Gr.4 and Gr.8 show a lower open-circuit voltage per cell of $V_{oc|Gr.4} = (659 \pm 5)$ mV cell^{-1} or $V_{oc|Gr.8} = (663 \pm 6)$ mV cell^{-1}, respectively. Hence, Ag front contacts cause a decrease in open-circuit voltage of $\Delta V_{oc} \approx 50$ mV compared to grid-free CIGS modules. Silver in pinholes of the CIGS layer may cause small shorts between the front and back contacts or an incorrect P3 scribing process resulting in shunts is a potential reason for this open-circuit voltage drop. Thermal damage in the CdS/CIGS interface cannot explain the different open-circuit voltages because the same curing treatment was carried out with all small-sized CIGS modules. The average open-circuit voltages are comparable within each category of applied contact grid independent of different cell widths.

However, if the open-circuit voltages of the modules are considered, evident differences between the various cell widths can be observed. Decreasing the number of cells in one small-sized CIGS module causes a decrease of the open-circuit voltage as well. The open-circuit voltage decreases from $V_{oc,module|Gr.8} = (19.23 \pm 0.17)$ V in group Gr.8 to $V_{oc,module|Gr.10} = (4.62 \pm 0.07)$ V in group Gr.10 where the cell width is $w_c = 16.857$ mm. Following, the increased cell width in combination with front contact metallization enables lower open-circuit voltages and hence an advantageous reduction in balance of system (BOS) costs.[16,33] Hence, the fabrication of CIGS modules needs to become more cost-competitive with state-of-the-art silicon modules.[34]

In general, the data suggest that wider cells in CIGS modules decrease the fill factor (FF) (Figure 4, bottom left). Nevertheless, the FF varies greatly between all experimental groups of this study. The grid-free CIGS modules have a significantly lower FF compared to metalized CIGS modules. The metallization of CIGS modules, which consists of 4.069 mm cells, already enables a FF gain of $\Delta FF_{rel.} = +27\%$ compared to grid-free CIGS modules. This FF advantage gets even more prominent when using broader cells in the CIGS modules. Grid-free CIGS

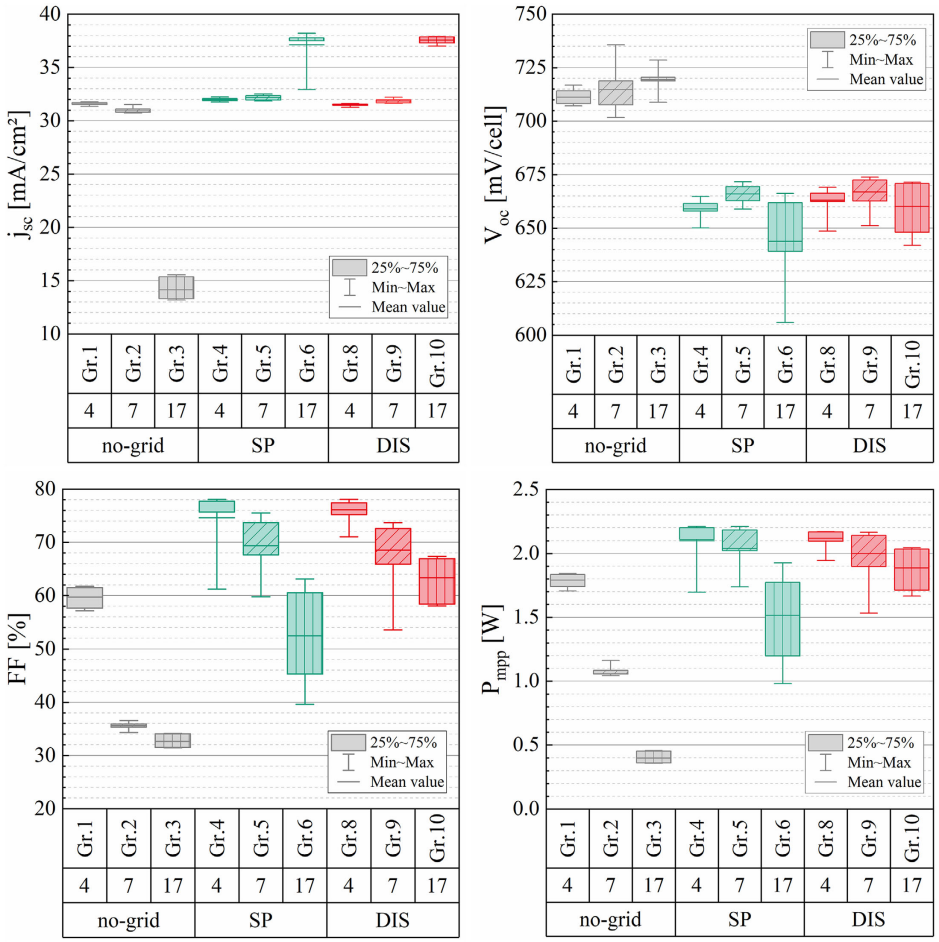

Figure 4. Electrical performance of small-sized CIGS modules measured by h.a.l.m. flasher *I-V*-tool at standard conditions. The small-sized CIGS modules are nonlaminated. The j_{sc}, V_{oc}, FF, und P_{mpp} values are depicted for the different experimental groups, which differ regarding their cell width w_c ($w_c = 4.069$ mm, $w_c = 6.941$ mm, $w_c = 16.857$ mm) and metallization technique (SP = flatbed screen printing; DIS = parallel dispensing).

modules that consist of 16.857 mm wide cells have an average FF of $FF_{Gr.3} = (32.64 \pm 1.19)\%$. Comparing the two metallization technologies, a similar level of the FF at $FF_{Gr.4} = (74.60 \pm 5.54)\%$ and $FF_{Gr.8} = (76.10 \pm 2.14)\%$ has been achieved for CIGS modules with 4.069 mm wide cells. However, the FF differs for CIGS modules with cells of $w_c = 16.857$ mm and both metallization techniques. With dispensed metal grids, an increase in FF of $\Delta FF_{rel.} = +21\%$ compared to CIGS modules with screen-printed metal grids ($FF_{Gr.6} = (52.45 \pm 7.77)\%$; $FF_{Gr.10} = (63.38 \pm 3.54)\%$) has been achieved. In addition, the average FF of $FF_{Gr.10} = (63.38 \pm 3.54)\%$ is even higher than the FF of grid-free CIGS modules and 4.069 mm cells ($FF_{Gr.1} = (59.73 \pm 1.95)\%$).

The presented tendencies of short-circuit current densities j_{sc}, open-circuit voltage V_{oc}, and fill factor FF are also evident in the aperture module efficiency $\eta_{ap.,module}$ and maximum module point P_{mmp} of each experimental group. Our results correspond to other published trends that evaluate the impact of metal grids as front contacts on CIGS modules. Other publications can confirm our study results.[9,11,21,22] The module power P_{mmp} decreases when the cell width increases as suggested by Figure 4 at the bottom right. This trend is most prominent for grid-free modules. In this case, the average maximum module power point loses down to $\Delta P_{mmp,rel.} = -78\%$. Grid-free CIGS modules which consist of 4.069 mm cells have an average aperture module efficiency of $\eta_{ap.,module|Gr.1} = (12.19 \pm 0.38)\%$ and an average module power of $P_{mpp,Gr.1} = (1.79 \pm 0.06)$ W. Small-sized CIGS modules with screen-printed and dispensed metal grids have comparable aperture module efficiencies $\eta_{ap.,module}$ and maximum power points of $P_{mmp|Gr.4} = (2.10 \pm 0.17)$ W ($\eta_{ap.,module|Gr.4} = (14.64 \pm 0.67)\%$) and $P_{mmp|Gr.8} = (2.12 \pm 0.07)$ W ($\eta_{ap.,module|Gr.8} = (14.35 \pm 0.71)\%$) for narrow cell widths. The module performance increases up to $\Delta P_{mmp,rel.} = +18\%$, when a front contact metallization onto the ITO layer is applied compared to grid-free CIGS modules. The advantage of dispensed metal grids is obvious for 16.857 mm cells in CIGS modules compared to screen-printed metal grids. CIGS modules of group Gr.6 show an average aperture module efficiency of $\eta_{ap.,module|Gr.6} = (9.79 \pm 1.89)\%$, CIGS modules of group Gr.10 have an average aperture module efficiency of $\eta_{ap.,module|Gr.10} = (12.19 \pm 0.90)\%$. The module performance increases by $\Delta P_{mmp,rel.} = +25\%$ when applying a dispensed metal

grid. One reason for this result is the printed Ag-electrodes' homogeneity, particularly the low deviation in electrode height. Screen-printed structures show mesh marks caused by wires in the screen, resulting in a strong variation of electrode height.[35] However, dispensed Ag-electrodes deviate only slightly in height, resulting in a more effective Ag consumption regarding electrical conductivity per milligram of silver. In previous studies, microscope images illustrate this difference.[19,28] It is expected that the electrode pitch differences of $\Delta = 0.012$ mm do not cause this difference in module performances for both metallization technologies. The front contact metallization enables CIGS module designs with wide cells, especially dispensed Ag-electrodes. Following this, the number of cells, including the amount of scribing and the dead area of the active module, is minimized from 29 cells per small-sized CIGS module to 7 cells per small-sized CIGS module. Hence, the areal percentage by P1P2P3 interconnections decreases from $A_{P1P2P3} = 7.19\%$ per module to $A_{P1P2P3} = 1.74\%$.

In this case, the screen-printed Ag-electrodes have core electrode widths of $w_{core} = (30 \pm 2)$ µm and optical aspect ratios of $AR_o = 0.31 \pm 0.04$. Compared to that, dispensed Ag-electrodes show core electrode widths of $w_{core} = (46 \pm 1)$ µm and optical aspect ratios of $AR_o = 0.31 \pm 0.01$. In addition, the TLM measurements result in comparable contact resistivities $\rho_{c,TLM}$ and sheet resistances $R_{sh,TLM}$ for screen-printed and dispensed Ag-electrodes on the ITO layer (**Figure 5**). TLM substrates of group Gr.7 present an average contact resistivity of $\rho_{c,TLM|Gr.7} = (1.8 \pm 1.7)$ m Ω cm^2 and a sheet resistance of $R_{sh,TLM|Gr.7} = (78 \pm 6)$ Ω sq^{-1}. The dispensed Ag-electrodes achieve an average contact resistivity of $\rho_{c,TLM|Gr.11} = (2.2 \pm 2.2)$ m Ω cm^2 and a sheet resistance of $R_{sh,TLM|Gr.11} = (75 \pm 6)$ Ω sq^{-1}.

The effective area per module A_{eff} is obtained from the difference between the aperture area per module $A_{aperture}$ and the lost area per module A_{lost}. The relative loss of effective area per small-sized CIGS module A_{lost} is calculated for different module designs. An interconnection width of $w_{P1P2P3} = 300$ µm and Ag-electrode width of $w_{shading|SP} = 40$ µm or rather $w_{shading|DIS} = 57$ µm are estimated to determine the resulting loss of effective area per module A_{lost}. The lost area A_{lost} is defined as the proportion of the aperture module area $A_{aperture}$ that results from the scribing areas of P1P2P3 (= dead area) and the shading area of the front-side metallization. In **Figure 6**, the reference point in the origin is defined as group Gr.1 (grid-free, $w_c = 4.069$ mm). The area highlighted in red corresponds to a decrease in the effective area $\Delta A_{eff,rel.}$ as well as a decrease in the module performance $\Delta P_{mpp,rel.}$ The best-case scenario is visualized by the area highlighted in green which means that all these data points have a higher module performance P_{mpp} and a larger effective area per module A_{eff}. Data points in the other two quadrants of Figure 6 show either improvements of the effective area per module $\Delta A_{eff,rel.}$ or the module performance $\Delta P_{mpp,rel.}$, resulting in no decisive improvement.

On the one hand, the effective area of grid-free CIGS modules increases from $\Delta A_{eff,rel.|4\,mm} = 0\%$ to $\Delta A_{eff,rel.|17\,mm} = 6.3\%$ when increasing the cell width w_c. However, that results also in a significant loss in module performance by $\Delta P_{mpp,rel.} = -77.7\%$. On the other hand, the application of front contact metallization decreases the effective area by $\Delta A_{eff,rel.} = -4.7\%$ due to shading losses. However, an evident higher module performance compared to grid-free CIGS modules is achieved as the ITO layers regarding their electrical conductivity are better exploited. The module performance of metalized modules is improved up to $\Delta P_{mpp,rel.} = +18.4\%$. The optimization trade-off of effective area per module and module performance is realized by small-sized CIGS modules with 16.857 mm cells and dispensed Ag-electrodes. In this case, the effective area is slightly improved to $\Delta A_{eff,rel.} = +1.6\%$ and the power output of the CIGS modules to $\Delta P_{mpp,rel.} = +5.4\%$ compared to the reference point.

It should be noted that the proportion of shading losses resulting from the metal grid can be further optimized. First,

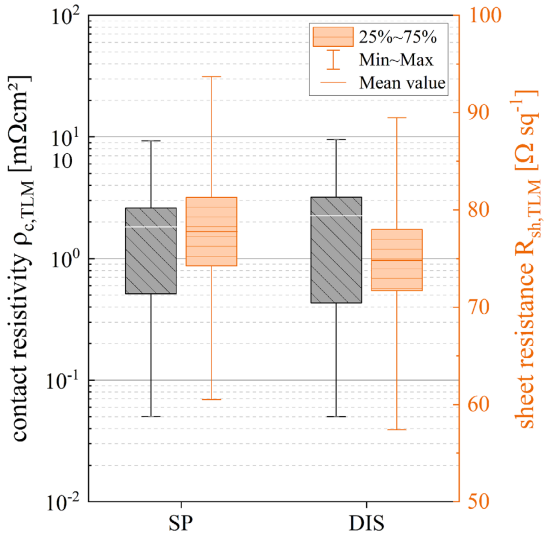

Figure 5. Contact resistivity $\rho_{c,TLM}$ and sheet resistance $R_{sh,TLM}$ of screen-printed and dispensed Ag-electrodes on CIGS substrates by TLM Scan from pv-tools GmbH.

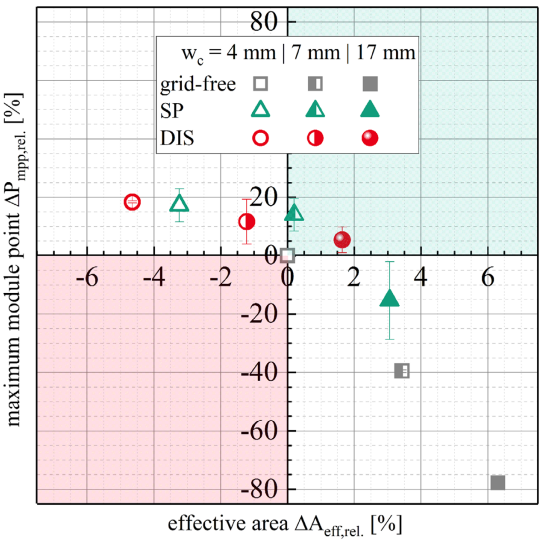

Figure 6. Module performance P_{mpp} plotted against effective area per module A_{eff}. An interconnection width of $w_{P1P2P3} = 300$ µm and the shading Ag-electrode widths $w_{shading}$ (results of the present experiment) are used to calculate the data points. Here, the grid-free small-sized CIGS modules with 4.069 mm cells are used as the initial point (data point in the origin).

the Ag-electrode widths can be reduced by adjustments in the printing processes. The potential of fine-line metallization was shown for silicon photovoltaics in the last decade.[24,36] Second, the design of the front contact metallization can also be adapted. In addition, the laser processes for scribing P1P2P3 can be improved to reduce the dead area of CIGS modules.

4. Conclusion

The thin-film CIGS concept requires metallization approaches that can cost-effectively realize a high-efficiency potential and thus increase the overall market share of the technology. In this study, the CIGS module architecture is varied regarding the cell widths of $w_c = 4.069$ mm, $w_c = 6.941$ mm, and $w_c = 16.857$ mm. Screen-printed and dispensed Ag-electrodes are applied onto these different CIGS module designs. Finally, the module performances of the grid-free, screen-printed and dispensed small-sized CIGS samples are compared. Applying a metal grid onto the ITO layer of CIGS modules decreases the open-circuit voltage down to $V_{oc} = (644 \pm 20)$ mV cell^{-1}, thus lowering BOS costs. CIGS modules which consist of 4.069 mm wide cells and a front contact metallization show an increase in module performance by $\Delta P_{mmp,rel.} = +18\%$ even though the relative loss of effective area on the module has been increased by $\Delta A_{lost} = +4.3\%$. The advantage of a front contact metallization on the ITO layer is even more evident for wider cells of $w_c = 16.857$ mm, resulting in aperture efficiency gains of $\Delta \eta_{ap.,module} = +373\%$ and module performance gains of $\Delta P_{mmp,rel.} = +373\%$ compared to grid-free CIGS modules. In addition, the homogeneous Ag-electrodes by parallel dispensing show a further increase in module performance of $\Delta P_{mmp,rel.} = +25\%$ compared to screen-printed contacts. This result demonstrates that front contact metallization onto CIGS modules enables wider cell widths and thus increases the effective active module area. This shows the great potential of combining the dispensing technology for front contact metallization with the CIGS concept. In the future, the increase in module performance can be further improved when applying paste systems that enable a contact formation at lower temperatures because temperature-based damages of the CIGS substrates and thus losses in open-circuit voltage may be reduced or even completely prevented.

Acknowledgements

This work was supported by the German Federal Ministry for Economic Affairs and Energy within the research project "Altura" under the contract number 03EE1006C. The authors would like to thank NICE Solar Energy GmbH for providing CIGS samples and for characterization of small-sized CIGS modules. A special thanks goes to Philipp Köder, Niccola Zancan, Hans-Peter Kurz, and Joachim Müller. The authors are responsible for the content.

Open Access funding enabled and organized by Projekt DEAL.

Conflict of Interest

The authors declare no conflict of interest.

Data Availability Statement

Research data are not shared.

Keywords

Ag pastes, CIGS, dispensing, solar cell metallization, thin-film photovoltaics

Received: February 3, 2022
Revised: April 4, 2022
Published online: May 20, 2022

[1] L. Zortea, S. Nishiwaki, T. P. Weiss, S. Haass, J. Perrenoud, L. Greuter, T. Feurer, G. Palaniswamy, S. Buecheler, A. N. Tiwari, *Sol. Energy* **2018**, *175*, 25.
[2] R. Carron, S. Nishiwaki, T. Feurer, R. Hertwig, E. Avancini, J. Löckinger, S.-C. Yang, S. Buecheler, A. N. Tiwari, *Adv. Energy Mater.* **2019**, *9*, 1900408.
[3] M. O. Reese, S. Glynn, M. D. Kempe, D. L. McGott, M. S. Dabney, T. M. Barnes, S. Booth, D. Feldman, N. M. Haegel, *Nat. Energy* **2018**, *3*, 1002.
[4] (Eds: V. Petrova-Koch, R. Hezel, A. Goetzberger), *High-Efficient Low-Cost Photovoltaics: Recent Developments*, Springer, Berlin **2019**.
[5] CIGS White Paper 2019. https://cigs-pv.net/wortpresse/wp-content/uploads/2019/04/CIGS_White_Paper_2019_online.pdf (accessed: 8 December 2021).
[6] S. Yoshida, Solar Frontier Achieves World Record Thin-Film Solar Cell Efficiency of 23.35%. http://www.solar-frontier.com/eng/news/2019/0117_press.html (accessed: 22 June 2020).
[7] S. Enkhardt, Manz-Joint-Venture Nice Solar Energy vermeldet Wirkungsgradrekord von 17,6 Prozent für CIGS-Module, **2019**. https://www.pv-magazine.de/2019/12/04/manz-joint-venture-nice-solar-energy-vermeldet-wirkungsgradrekord-von-176-prozent-fuer-cigs-module/ (accessed: 4 April 2022).
[8] V. Bermudez, A. Perez-Rodriguez, *Nat. Energy* **2018**, *3*, 466.
[9] D. Herrmann, P. Kratzert, S. Weeke, M. Zimmer, J. Djordjevic-Reiss, R. Hunger, P. Lindberg, E. Wallin, O. Lundberg, L. Stolt, in *2014 IEEE 40th Photovoltaic Specialist Conf. (PVSC)*, IEEE, Denver, CO, USA, June 2014, pp. 2775–2777.
[10] O. Lundberg, E. Wallin, V. Gusak, S. Sodergren, S. Chen, S. Lotfi, F. Chalvet, U. Malm, N. Kaihovirta, P. Mende, G. Jaschke, P. Kratzert, J. Joel, M. Skupinski, P. Lindberg, T. Jarmar, J. Lundberg, J. Mathiasson, L. Stolt, *2016 IEEE 43rd Photovoltaic Specialists Conf. (PVSC)*, IEEE, Piscataway, NJ **2016**, pp. 1293–1296. https://doi.org/10.1109/PVSC.2016.7749824.
[11] M. Hedayati, S. Olyaee, *Opt. Quantum Electron.* **2020**, *52*, 346.
[12] VDMA Photovoltaics Equipment, International Technology Roadmap for Photovoltaics (ITRPV): Eleventh Edition, **2020**.
[13] P. Baliozian, S. Tepner, M. Fischer, J. Trube, S. Herritsch, K. Gensowski, F. Clement, S. Nold, R. Preu, *Proc. 37th European Photovoltaic Solar Energy Conf. and Exhibition*, Lisbon, Portugal, **2020**, pp. 420–426. https://doi.org/10.4229/EUPVSEC20202020-2CV.1.59.
[14] B. Retterstol Olaisen, S. Woldegiorgis, P.-O. Westin, M. Edoff, L. Stolt, A. Holt, E. Stenrud, *Technical Digest of the 15th Inter. Photovoltaic Science and Engineering Conf.*, Shanghai, China, **2005**.
[15] B. R. Olaisen, M. Edoff, A. Holt, *Proc. 24th European Photovoltaic Solar Energy Conf. and Exhibition*, Hamburg, Germany, **2009**.

[16] T. Freund, N. Zancan, G. Kaune, W. Bromenne, R. Wächter, T. Repmann, K. Orgassa, *37th European Photovoltaic Solar Energy Conf. and Exhibition*, Lisbon, Portugal, **2020**.
[17] J. D. Fields, G. Pach, K. Horowitz, T. R. Stockert, M. Woodhouse, M. van Hest, *Sol. Energy Mater. Sol. Cells* **2017**, *159*, 536.
[18] M. L. Crozier, P. Adamson, A. Brunton, S. Henley, J. D. Shephard, G. Kartopu, S. Irvine, P. M. Kaminski, J. M. Walls, *2014 IEEE 40th Photovoltaic Specialist Conf. (PVSC)*, IEEE, Piscataway, NJ **2014**, pp. 2784–2788. https://doi.org/10.1109/PVSC.2014.6925507.
[19] K. Gensowski, A. Jimenez, T. Freund, N. Wengenmeyr, S. Tepner, M. Pospischil, F. Clement, *Sol. RRL* **2020**, *4*, 2000475.
[20] A. Lachowicz, G. Christmann, C. Allebe, S. Nicolay, C. Ballif, in *2020 47th IEEE Photovoltaic Specialists Conf. (PVSC)*, IEEE, Calgary, AB, Canada, June 2020, pp. 261–262.
[21] Y. Li, S. Yang, X. Zhang, X. Xiao, *MRS Proc.* **2011**, *1315*, https://doi.org/10.1557/opl.2011.1393.
[22] J. van Deelen, C. Frijters, *Sol. Energy* **2017**, *143*, 93.
[23] M. Pospischil, Dissertation, Albert-Ludwigs-Universität, Freiburg im Breisgau, **2016**.
[24] M. Pospischil, T. Riebe, A. Jimenez, M. Kuchler, S. Tepner, T. Geipel, D. Ourinson, T. Fellmeth, M. Breitenbücher, T. Buck, M. Dhamrin, F. Clement, *AIP Conf. Proc.* **2019**, *2156*, 20005.
[25] M. Pospischil, M. Klawitter, M. Kuchler, M. Jahn, R. Efinger, R. Schwarz, L. Wende, M. König, F. Clement, D. Biro, *Energy Procedia* **2016**, *98*, 61.
[26] M. Pospischil, M. Klawitter, M. Kuchler, J. Specht, H. Gentischer, R. Efinger, M. Konig, M. Horteis, C. Mohr, L. Wende, J. Lossen, M. Weiss, O. Doll, I. Kohler, R. Zengerle, F. Clement, D. Biro, in *2013 IEEE 39th Photovoltaic Specialists Conference (PVSC)*, IEEE, Tampa, FL, USA, June 2013, pp. 2250–2253.
[27] D. Biro, J. Specht, D. Scheffler, M. Pospischil, F. Clement, EP 2 612 350 B1, **2013**.
[28] K. Gensowski, A. Jimenez, S. Tepner, E. Bujnoch, K. Muramatsu, M. Pospischil, F. Clement, *AIP Conf. Proc.* **2021**, *2367*, 020007.
[29] K. Gensowski, A. Jimenez, S. Tepner, M. Kuchler, M. Breitenbücher, T. Freund, P. Köder, J. Müller, B. Dimmler, M. Pospischil, F. Clement, *37th European Photovoltaic Solar Energy Conf. and Exhibition*, Lisbon, Portugal, **2020**.
[30] K. Gensowski, M. Much, E. Bujnoch, K. Muramatsu, M. Pospischil, S. Tepner, F. Clement, High-Speed Metallization on SHJ Solar Cells by Parallel Dispensing - Towards 650 mm/s Process Speeds at Line Widths Below 40 µm, 38th European Photovoltaic Solar Energy Conf. and Exhibition, Lisbon, Portugal, **2021**.
[31] S. Tepner, N. Wengenmeyr, L. Ney, M. Linse, M. Pospischil, F. Clement, *Sol. Energy Mater. Sol. Cells* **2019**, *200*, 109969.
[32] P. Hahne, Dissertation, FernUniversität Hagen, Hagen, **2020**.
[33] R. Wächter, G. Kaune, T. Repmann, K. Orgassa, *37th European Photovoltaic Solar Energy Conf. and Exhibition*, Lisbon, Portugal, **2020**.
[34] V. Bermudez, *Sol. Energy* **2017**, *146*, 85.
[35] S. Tepner, L. Ney, M. Singler, M. Pospischil, K. Masuri, F. Clement, *J. Comput. Sci.* **2021**, *51*, 101325.
[36] S. Tepner, L. Ney, M. Singler, R. Preu, M. Pospischil, F. Clement, *Sci. Rep.* **2021**, *11*, 4352.